Journal of Chromatography A, 1217 (2010) 4675–4681

Contents lists available at ScienceDirect

Journal of Chromatography A

journal homepage: www.elsevier.com/locate/chroma

Preparation of macroporous methacrylate-based monoliths for chromatographic applications by the Reactive Gelation Process

M. Bechtle[a], A. Butté[b], G. Storti[c], M. Morbidelli[a,*]

[a] Institute for Chemical and Bioengineering, Department of Chemistry and Applied Biosciences, ETH Zurich, 8093 Zurich, Switzerland
[b] LES R&D DSP Technologies, Lonza AG, 3930 Visp, Switzerland
[c] Dipartimento di Chimica, Materiali e Ingegneria Chimica "Giulio Natta", Politecnico di Milano, 20133 Milan, Italy

ARTICLE INFO

Article history:
Received 3 February 2010
Received in revised form 24 April 2010
Accepted 28 April 2010
Available online 6 May 2010

Keywords:
Reactive Gelation
Monoliths
PMMA
Protein purification
Downstream processing

ABSTRACT

Polymeric monoliths are a relatively new separation medium for chromatographic applications. The innovative approach to produce such monoliths, the Reactive Gelation Process, presented by Marti et al. [1] for polystyrene macroporous materials is applied to a methacrylate-based material. It is shown that it is possible to create a macroporous structure by Reactive Gelation also with this polymer even if the properties of the material are different. Besides the analysis of the material by SEM and BET, several chromatographic methods are used to analyze the material properties. The ISEC experiments showed a much smaller size exclusion effect than in conventional packed beds. The permeability of the material is comparable to a packed bed with 4.13 μm particles. The column efficiency is not changing for increasing flow rates. Because of the high efficiency of the material, shorter columns are needed and therefore the comparatively low permeability is compensated. The monolith also exhibits a significant adsorption capacity for hydrophobic interaction, which makes it suitable for chromatographic purification processes.

1. Introduction

Macroporous polymer supports are widely used as stationary phase for chromatographic separation of biomolecules. Classically these supports are micrometer size macroporous particles. Whilst the technology for producing these particles is quite well assessed [2], chromatographic columns packed with such beads show some important limitations. Packed beds are characterized by a bimodal pore size distribution [3]: the small size mode is due to the intraparticle mesopores, which give access to the large surface area. The large size mode is due to the interparticle volume, through which the mobile phase flows by convection. To access the intraparticle mesopores, the solute must diffuse into the stagnant phase of the pores; such diffusion is very slow for solutes of large molecular size, as it is the case for most biomolecules. This leads to low column efficiency and hence to low productivity of the separation process. One solution could be to decrease the particle size thus reducing the characteristic length for diffusion. To increase column efficiency significantly, submicron particles should be adopted. However, such small particles would decrease the permeability of the column, thus increasing the corresponding pressure drop. Therefore very small particle sizes are not feasible for industrial applications. Classically, polymeric porous materials are produced by suspension polymerization in the presence of porogens [4]. This process has a main drawback: the pore size distribution is difficult to control and micropores are always formed [5]. The pore formation is controlled by temperature, amount and type of porogen and amount of crosslinker, but the complex interplay among all these parameters is not always fully understood. This leads to another limitation of columns packed with polymeric material, which is made with porogens: the size exclusion effect. In fact, the intraparticle mesopores show a certain pore size distribution and therefore bigger molecules are excluded from smaller pores, while small molecules are still able to enter. This leads to a significant loss of surface area for adsorption of large molecules.

In order to overcome these limitations, the use of monoliths as separation media has been proposed [6,7,3]. In this case all the liquid percolates through the pores, where surface for adsorption is mainly located. Several studies show higher permeability and faster mass transfer for this relatively new kind of stationary phase [8]. If these monoliths are produced by bulk polymerization in a one step process the ability to scale up monolithic columns is limited. The dissipation of the polymerization heat becomes limiting at increasing diameter of the cylindrical monolith, which leads to temperature hot spots and thus to non-homogeneities in the final structure [9]. The mechanism of pore formation in monoliths

* Corresponding author. Tel.: +41 446323034.
E-mail address: massimo.morbidelli@chem.ethz.ch (M. Morbidelli).

0021-9673/$ – see front matter © 2010 Elsevier B.V. All rights reserved.
doi:10.1016/j.chroma.2010.04.077

produced by bulk polymerization is the same as for macroporous particles, since a porogen is used similary, and therefore these monolithic columns show the same loss of surface area for adsorption of large molecules as columns packed with macroporous beads made with porogens.

Marti et al. [1] developed a new approach to synthesize macroporous polymeric materials, the so-called 'Reactive Gelation' Process. This process comprises three independent steps: the formation of monodisperse polymer particles by (mini)emulsion polymerization, the macroporous network formation by gelating the latex and the gel post-polymerization to 'freeze' the fractal structure of the gel and impart mechanical strength to the material. By splitting the synthesis of the material into three steps instead of polymerizing it just in one step, it was possible to overcome the two mentioned drawbacks of forming a macroporous polymeric monolith by bulk polymerization. Polymer gels are made of clusters of latex particles [10] aggregated with a fractal structure [11], so the pores (which are constituted by the voids among the gelated latex particles) are formed during this step. By changing the particle size, the polymer composition, the particle morphology, their surface characteristics and functionalities in the emulsion polymerization step and the gelation speed during the gelation step independently from each other, the pore formation can be controlled in a very defined way. About 80% of the polymer mass is produced by emulsion polymerization, where the removal of the heat of polymerization is easy [12]. In the post-polymerization, where the rest of the polymer mass is produced, 90% of the gel consists of water, which has a high heat capacity and acts as a heat sink: therefore much bigger monoliths can be produced without problems of heat removal [13].

While Marti et al. were focused on polystyrene monoliths, this paper reports the synthesis of poly(methyl methacrylate-co-ethylene dimethacrylate) (P(MMA-co-EDM)) material. In fact methacrylate-based polymers are much less hydrophobic than polystyrene and therefore more suitable for bio-oriented applications such as protein purification [14,15]. Another key difference compared to [1] is the packing of the material: it is not ground anymore to be used as a packed bed but a self-sealing fitting ring is assembled around the macroporous material, to use the monolith in a suitable housing.

2. Experimental

2.1. Instrumentation

Miniemulsion polymerization was carried out with a Mettler Toledo LabMax Automatic Reactor in a 4 L jacketed glass reactor. The miniemulsion was produced with a Hielscher UP400S ultrasonic processor. Dry solid fraction of the latex was measured gravimetrically with a Mettler Toledo HG53 Moisture Anaylzer. The particle size of the initial latex was determined by dynamic light scattering in a Malvern Zetasizer Nano ZS. The total surface for adsorption was determined by N_2 adsorption using the BET algorithm with a Micromeritics Tristar Series 320. Scanning Electron Microscopy was performed with a Zeiss Gemini 1530 field emission microscope. To use the monolith in a HPLC system, a Bia Separations CIM® Disk Housing was used. The chromatographic measurements were carried out on a Agilent HPLC 1100 Series. The instrument is equipped with UV and refractive index detectors. The pressure drop over the monolithic column was determined with a GE Healthcare ÄKTA basic equipment (pump P-900, UV-900, pH/C-900). The pressure sensor was located directly at the pump outlet, being the outlet of the column open to atmosphere.

2.2. Materials

Methyl methacrylate (MMA), 2, 2′-azobis(2-methylpropionitrile) (AIBN), sodium dodecylsulfate (SDS), D.E.R. 332 epoxy resin, tetraethylenepentamine (TEP), thiourea and dextran standards were purchased at Fluka (Buchs, Switzerland). Ethylene glycol dimethacrylate (EGDM), sodium dihydrogen phosphate (NaH_2PO_4) were purchased at Merck (Darmstadt, Germany). n-Hexadecane (HD), sodium phosphate dibasic (Na_2HPO_4) and ammoniumsulfate ($(NH_4)_2SO_4$) were obtained from Acros Organics (Geel, Belgium). Sodium chloride (NaCl) was purchased at J.T. Baker (Deventer, Netherlands). Gammanorm is human normal immunoglobulin gamma (IgG) with an IgG content of >95% in solution (165 g/L) and was obtained from Octapharma (Stockholm, Sweden). All chemicals have been used without further purification. Ultra-pure grade water has been prepared by purifying deionized water with a Simpak 2 unit by Millipore.

2.3. Chromatographic columns

A weak cation exchange column Propac WXC-10 = 4 mm × 100 mm was purchased at Dionex (Sunnyvale, CA, USA). Fractogel® EMD SO_3^- (S), and Fractogel® EMD SO_3^- (M), donated by Merck (Darmstadt, Germany), was packed into Tricorn columns obtained from GE Healthcare (Chalfont St. Giles, UK). The columns have a inner diameter of 5 mm. 20% mechanical compression of the bed was applied to the resin. The column packed with Fractogel® EMD SO_3^- (S) had a length of 4 cm, the column packed with Fractogel® EMD SO_3^- (M) was 4.5 cm long.

2.4. Methods

2.4.1. Preparation of methacrylate monoliths by Reactive Gelation

The Reactive Gelation Process was carried out as described by Marti et al. [1]. To avoid unspecified sulfonic groups on the surface, the preparation of the initial latex was changed from emulsion polymerization with potassium peroxodisulfate as initiator to miniemulsion polymerization with the oil-soluble initiator AIBN [16].

Miniemulsion polymerization. The composition of the miniemulsion was according to the recipe in Table 1. The surfactant SDS was dissolved in water. MMA, EGDM, AIBN (as an oil-soluble initiator) and HD (as a hydrophobe) were mixed, added to the SDS solution and stirred for 1 h. This emulsion was sonicated in continuous mode at 360 W for 0.5 h. The reactor was charged with this miniemulsion and purged with several nitrogen/vacuum cycles. Afterwards the temperature was brought to reaction temperature and the reaction started. Samples were withdrawn with a syringe to measure both conversion gravimetrically and the particle size by dynamic light scattering. At 80% conversion the addition of the continuous feed with a low crosslinker concentration under starved conditions was started. Due to this feeding strategy particles with a hard core and a soft shell were produced.

Latex swelling and gelation. The latex was mixed with monomer, crosslinker and initiator in a 30 mL flat-bottom flask and swollen under stirring. The swelling fraction was 30% monomer/crosslinker with respect to the latex dry content. After 2 h, NaCl solution was added dropwise under vigorous stirring and the mixture was left at room temperature for 24 h to complete the gelation. The amount of salt solution for the gelation was calculated to get a final dry content in the gel of 10%.

Post-polymerization. The flask was put into an oil-bath at 55 °C and left polymerizing for 8 h. After cooling it down, the supernatant water was removed and the monolith was washed 3 times with water and 3 times with methanol to remove salt and unreacted monomer. Finally it was slowly dried at room temperature.

Table 1
Recipe for the production of monoliths by the Reactive Gelation Process.

	Initial charge	Continuous feed	Swelling	Gelation	Post-polymerization
Water/g	2800	–	–	–	–
MMA/g	281	349.13	0.27	–	–
EGDM/g	69	0.88	0.03	–	–
SDS/g	10.5	–	–	–	–
HD/g	14	–	–	–	–
AIBN/g	7.00	–	0.003	–	–
Latex/g	–	–	5	–	–
NaCl sol., 0.2125 M/g	–	–	–	5	–
Duration/h	1	7	2	24	8
Temperature/°C	55	55	25	25	55
Particle size/nm	114	134	–	–	–
Dry solid fraction/%	9.65	19.84	19.84	10	10

Packing. To be used in a HPLC system the monolith has to be "packed" into a column. To arrange it into a CIM® Disk Housing, a self-sealing fitting ring was assembled around the monolith. The monolith was first dressed to the right size (12 mm in diameter) and the sealing ring was assembled by casting a mixture of 80 wt% D.E.R. 332 (resin) and 20 wt% TEP (curing agent) around the monolith. The resulting monolith (macroporous structure plus non-porous fitting ring) was dressed to a diameter of 16 mm.

2.4.2. Pore structure by Scanning Electron Microscopy

The material was ground and a small amount of it was placed on a specimen mount. The samples were investigated as prepared at low voltage (1 kV).

2.4.3. Total surface

The total surface of the ground material available for adsorption was measured by adsorption/desorption of nitrogen and transformed into a specific surface area by the Brunauer–Emmett–Teller equation [17].

2.4.4. Porosity by Inverse Size Exclusion Chromatography

Inverse Size Exclusion Chromatography (ISEC) was used to determine the pore size distribution of the material by monitoring the elution time t of solutes of varying molecular diameter under non-adsorbing conditions [18]. The elution time was determined by the zero-th and first order moments of the peak [19]:

$$t = \frac{\mu_1}{\mu_0} \tag{1}$$

The corresponding porosity ϵ was calculated by

$$\epsilon = \frac{F \cdot t}{V_{\text{monolith}}} \tag{2}$$

where F is the volumetric flowrate and V_{monolith} is the monolith volume. The following dextran standards with different molecular weights (Da) were used as probing solutes (in parentheses the corresponding hydrodynamic radius in nm [20]): $\bar{M}_n$ = 5000 (1.88), 12,000 (2.91), 50,000 (5.93), 150,000 (10.25), 410,000 (16.91). The column total porosity was determined by using thiourea as tracer. A 50 mM sodium phosphate buffer at pH 8 was used as eluent with a superficial velocity of 0.53 cm/min.

2.4.5. Pore diffusivity

To analyse the diffusion phenomena in the monolith, the van Deemter plot was evaluated. In this plot the Height Equivalent to a Theoretical Plate, HETP, is plotted versus the interstitial velocity u (defined as $u = u_{\text{lin}}/\epsilon_e$) of the eluent. The van Deemter equation [21]

$$\text{HETP} = A + \frac{B}{u} + C \cdot u \tag{3}$$

couples the column efficiency (in terms of HETP) to molecular diffusion (A), axial dispersion (B) and pore diffusion (C). Because the peak shape was not symmetric due to large hydrodynamic non-idealities of the CIM® Disk Housing, the HETP-value was calculated directly from the first order moments of the peak [22]:

$$\text{HETP} = \frac{\sigma^2}{t^2} \cdot L \tag{4}$$

where L is the monolith length, the retention time t is given by Eq. (1) and the variance σ^2 by:

$$\sigma^2 = \frac{\mu_2}{\mu_0} - \left(\frac{\mu_1}{\mu_0}\right)^2 \tag{5}$$

Since higher moments are very sensitive to measurement errors and signal noise, the experimentally obtained peaks were fitted by a perturbed Gamma distribution [23] before the HETP-value was calculated. Under linear adsorption conditions, the variances of the peak are additive [24], i.e. the overall peak broadening is the additive result of the broadening effects of the different elements of the system:

$$\sigma^2_{\text{total}} = \sum_i \sigma_i^2 = \sigma^2_{\text{monolith}} + \sigma^2_{\text{HPLC}} \tag{6}$$

where $\sigma^2_{\text{monolith}}$ represents the peak variance caused by the monolith and σ^2_{HPLC} refers to the contribution of the HPLC system (including capillaries, pump, detector, CIM® Disk Housing, etc.) to the peak broadening. The experiments were conducted the same way as the ISEC experiments, but with a variation of the interstitial velocity between 0.18 cm/min and 3.63 cm/min. To eliminate the influence of the hydrodynamic non-idealities of the CIM® Disk Housing, these experiments were repeated with the empty housing to obtain σ^2_{HPLC} which was, according to Eq. (6), substracted from the overall variance σ^2_{total} to determine the performance of the monolith itself.

2.4.6. Average pore size for convection

To maintain a constant flowrate through the column, a certain pressure drop ΔP has to be overcome. By assuming a Newtonian behavior of the mobile phase and laminar flow, ΔP can be expressed by the Darcy's law [25]:

$$\Delta P = \frac{\eta u_{\text{lin}} L}{B} \tag{7}$$

where η is the dynamic viscosity of the mobile phase, u_{lin} the superficial velocity (ratio of flow rate and column cross-section area), L the length of the monolith and B is the column permeability. In the case of packed columns, the permeability of the column is related to the average diameter of the packing particles d_p by

$$B = k_F d_p^2 \tag{8}$$

where k_F is the specific permeability of the packed bed [19]. To fairly compare a monolithic column with a packed column, it is common practice to determine an equivalent average particle size which would give the same permeability as the monolithic column. The Kozeny–Carman equation

$$k_F = \frac{\epsilon_e^3}{180(1-\epsilon_e)^2} \quad (9)$$

relates the specific permeability to the external porosity ϵ_e of a packed bed.

Water was pumped through the monolith with superficial velocities varying between 0.71 cm/min and 3.54 cm/min and the back pressure of the system was recorded. B was obtained from the slope of the specific pressure drop $\Delta P/L$ versus u_{lin}.

2.4.7. Adsorption behavior

The adsorption behavior of the P(MMA-co-EDM) matrix was evaluated by hydrophobic interaction chromatography (HIC). In a first evaluation, the batch adsorption capacity of the material was determined. In a second experiment, the adsorption behavior under chromatographic (dynamic) conditions was examined.

Batch adsorption. Approx. 20 mg of ground stationary phase was mixed in HPLC vials with 1 mL 50 mM sodium phosphate buffer containing 0.5 M and 1 M $(NH_4)_2SO_4$ respectively. Different amounts of IgG were added to each vial and the system was equilibrated overnight while shaking. After the solid settled down, the IgG concentration of the supernatant solution was analyzed with a weak cation exchange column Propac WCX-10 = 4 mm × 100 mm under non-adsorbing conditions. The sample concentration was correlated to the peak area by calibration with samples of known concentrations.

Overloaded gradient elution. Different amounts of IgG were adsorbed at a high salt concentration during 7 min and eluted by applying a solvent gradient to a low salt concentration over 20 min. For adsorbing conditions a 50 mM sodium phosphate buffer containing 1 M $(NH_4)_2SO_4(NH_4)_2SO_4$ at pH 8 was used. In the gradient elution step, a 50 mM sodium phosphate buffer with no salt was mixed to this buffer at increasing ratio. Such experiments were run with a superficial velocity of 0.44 cm/min.

3. Results and discussion

3.1. Material properties

For a qualitative analysis of the morphology of the material, SEM pictures were visually analyzed. The SEM picture of the material obtained by the recipe reported in Table 1 is shown in Fig. 1. The latex particles can still be identified and it can be confirmed that the original particle size was around 130 nm and the pore size appears to be on the lengthscale of μm. However the particles are fused into each other to a certain extent. In fact, the original latex particles had a specific surface area of 37.94 m^2/g (calculated by $6/\rho d_p$, where ρ is the polymer density and d_p is the particle diameter of the primary latex particles). According to the BET measurement of the final material, the specific surface area was reduced to 26.34 m^2/g which means that 31% of the starting surface is lost due to particle fusion.

The results of the ISEC experiments are shown in Fig. 2. Thiourea was used as a tracer to determine the overall porosity of 55%. Such value is much smaller than the one expected from the recipe: the polymer content in the gelation step was 10%, which means a void fraction of 90%. Therefore a significant loss of porosity is taking place during the post-polymerization. This behavior can be explained by the rearrangement of the latex particles during the post-polymerization, which results in shrinking of the monolithic

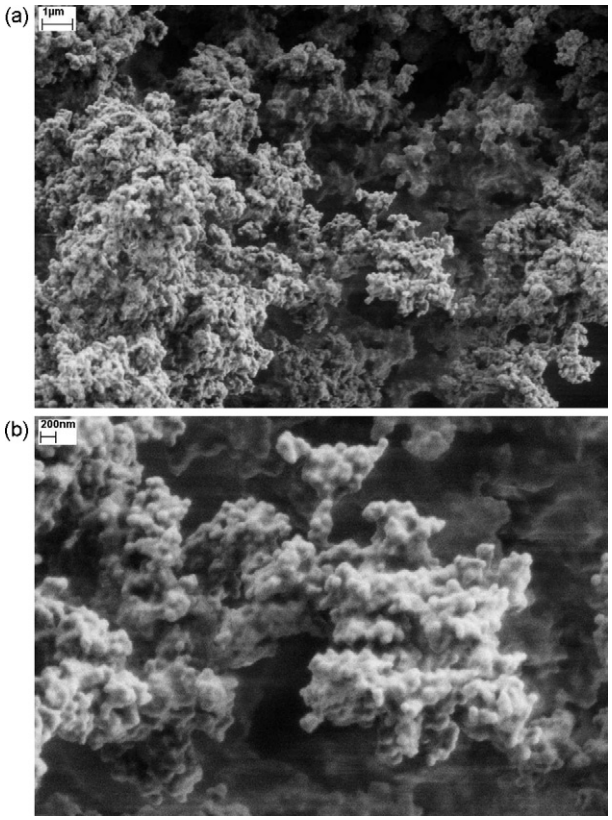

Fig. 1. SEM picture of the porous material. (a) The material is shown in the lengthscale of μm to see the overall structure. (b) The magnification is increased to observe the structure of the primary particles.

structure. The final monolith had approx. 40% less void volume compared to the initial gel.

To check the pore size distribution of the material, dextran standards with increasing molecular weight (i.e. increasing hydrodynamic radii) were injected and the retention time was monitored. Due to the decreasing retention time with increasing molecular weight, a limited size exclusion effect can be observed, which means that not all pores are large enough to be accessible for all molecule sizes. This behavior was compared to the data from

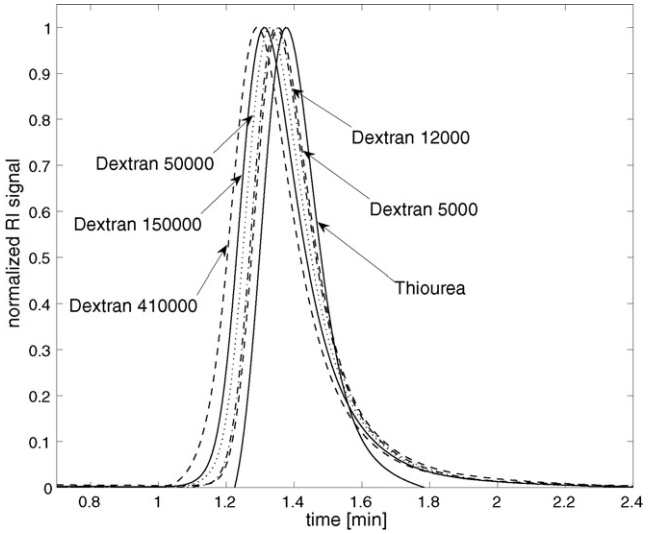

Fig. 2. Normalized UV signal as a function of the retention time obtained by ISEC experiments.

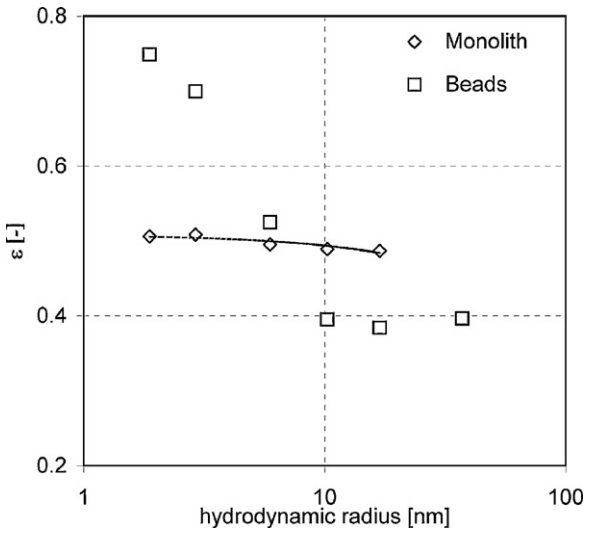

Fig. 3. Porosity of material depending on the tracer hydrodynamic radius: comparison between the monolithic material and commercial bead material (Fractogel® EMD SE Hicap (M))[26].

Franke et al. [26] for commercially available beads (Fractogel® EMD SE Hicap (M)). For both materials the associated porosity for the different tracer molecules was calculated and plotted versus the hydrodynamic radii of the tracer molecules in Fig. 3. Compared to the bead material, the size exclusion effect of the monolithic material is negligible, a clear advantage of the latter with respect to the conventional packing. Note that Fig. 3 does not cover the entire pore size distribution of the material, but only the portion of interest to investigate size exclusion effects of bio-molecules. In fact, as evident from Fig. 1, pores much larger than 100 nm are present in the material, which are instead interesting for determining the monolith permeability, as discussed below.

3.2. Hydrodynamic performance

The permeability of the monolithic column was obtained by applying Eq. (7). In Fig. 4 the specific pressure drop $\Delta P/L$ was plotted versus the superficial velocity u_{lin} and the slope of the line of best fit was determined. According to Eq. (7) this slope m corresponds to the permeability B as follows:

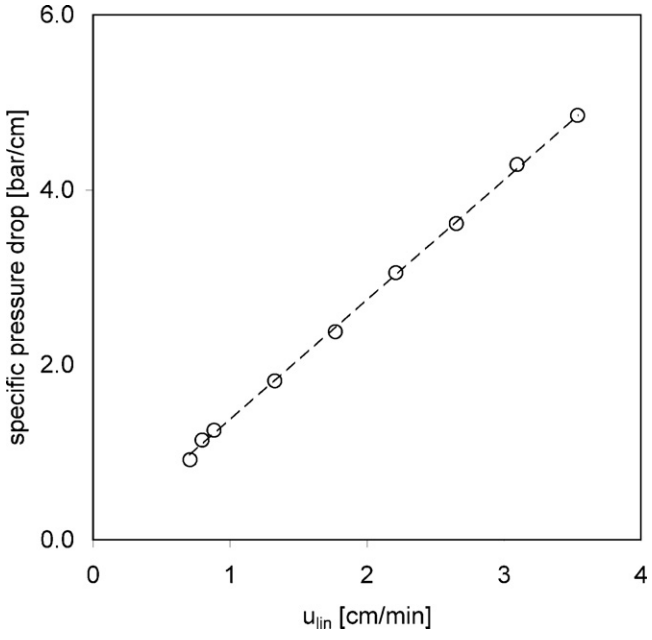

Fig. 4. Specific pressure drop $\Delta P/L$ as a function of the superficial velocity u_{lin}.

Table 2
Pressure drop as a function of NETP for monolith (12 mm × 13.5 mm) and Fractogel® EMD SO_3^- (S) (5 mm × 40 mm) and (M) (5 mm × 45 mm).

Fractogel® EMD SO_3^- (S)		Fractogel® EMD SO_3^- (M)		Monolith	
NETP	ΔP (bar)	NETP	ΔP (bar)	NETP	ΔP (bar)
35.06	4.7	39.49	2.6	437.58	0.3
29.73	6.6	23.88	4.4	411.25	0.3
29.1	8.6	21.45	6.1	387.39	0.5
28.29	10.4	19.82	7.9	331.63	0.7
		19.06	9.7	305.21	0.8

$$B = \frac{\eta}{m} \tag{10}$$

With a dynamic viscosity for water of 1×10^{-3} Pa s, the column permeability is estimated as 1.21×10^{-10} cm^2. For the determination of the equivalent particle diameter we assume a random close packing, with an external porosity ϵ_e of 0.37 [27]. According to Eq. (9) the corresponding specific permeability is 7.09×10^{-4} cm^2 and the equivalent particle diameter d_p from Eq. (8) is 4.13 μm. This means that a column packed with 4.13 μm particles has the same permeability as the monolith.

Let us now analyze the behavior of the monolith in terms of van Deemter plot. At higher interstitial velocities, the pore diffusion term becomes predominant in Eq. (3). Therefore, if the HETP value is linearly increasing at increasing interstitial velocity, the pore diffusion is the predominant contribution to the mass transport resistance. The analysis was carried out by injecting small amounts of the Dextran 150,000 standard under non-adsorbing conditions at linear velocities varying between 0.6 cm/min and 3 cm/min. As it can be seen in Fig. 5, the HETP for the PMMA monolith is 10 times smaller than the HETP values reported by Marti [28] for the PS-DVB monolith. In Fig. 5(a) the HETP of the monolith is compared to commercial bead materials (Fractogel® EMD SO_3^- (S) (d_p =20–40 μm) and (M) (d_p =40–90 μm)) and it becomes evident that the column efficiency of the PMMA monolith is 100 times higher. In addition, and even more important, the HETP of the PMMA monolith is not increasing for increasing velocities as it does for the other 3 materials. That means that the mass transport in the PMMA monolith is dominated by convection and not by diffusion. The tracer used for these experiments in PMMA was Dextran 150,000, a relatively large molecule which accesses large pores only. The results for the PS monoliths, which are also shown in Fig. 5, where obtained by using IgG as solute, which has a comparable size to Dextran 150,000. The fact that the HETP is increasing for increasing velocities in PS could be related to larger micropores present in the material, which are accessible for IgG. However, IgG is most probably adsorbing on PS, which means the increase in HETP can be related to the contribution of surface diffusion. Column efficiency and column permeability are not independent from each other. In a packed bed a high efficiency is paid by a low permeability. On the first glance it seems, that the permeability of the monolith is rather low, but in conjunction with its high efficiency, this evaluation is relativized.

In Table 2 the pressure drop is shown as a function of the NETP (number equivalent of theoretical plates, NETP = L/HETP) for the monolith and for Fractogel® EMD SO_3^- (S) and (M) materials with different particle sizes (20–40 μm and 40–90 μm respectively). It is evident that for a much higher number of theoretical plates the pressure drop of the monolith is much smaller than for the bead material. Both materials have much larger particle diameter than the equivalent particle diameter of the monolith (4.13 μm). Because of the very small HETP value of the monolith, a much shorter monolith length is required for a given separation efficiency

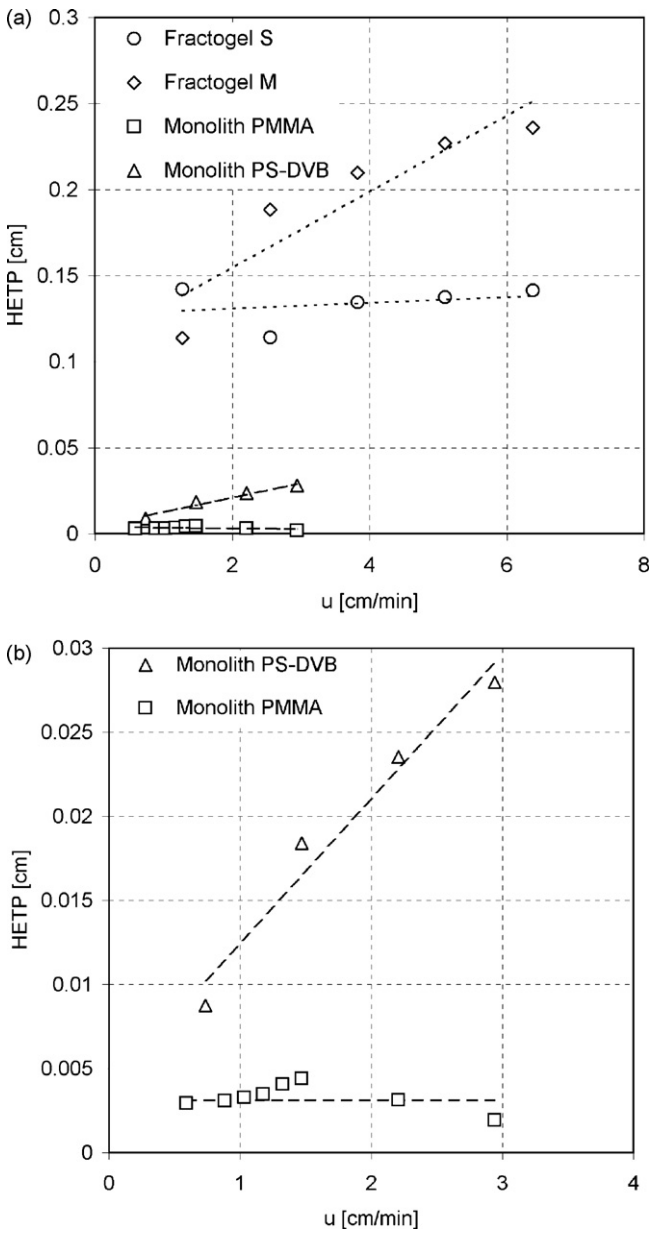

Fig. 5. van Deemter plot: comparison of the HETP versus interstitial velocity. (a) Between monoliths and Fractogel® SO_3^- (S) and (M), and (b) between PS-DVB and PMMA monoliths (data for PS-DVB monolith from [28]).

and hence the overall pressure drop is much smaller. This effect is also shown in Fig. 6. From the data in Table 2 for the interstitial velocity u =2.4 cm/min the column lengths to reach a given column efficiency (namely NETP values of 100, 500 and 1000) were calculated and transferred into the corresponding pressure drops. Whilst the column length for the bead material increases approx. from 15 cm to 150 cm and therefore the pressure drop increases from approx. 15 bar to 150 bar for an NETP increase from 100 to 1000, the monolith's length increases from 0.3 cm to 3 cm and therefore the pressure drop increases from 0.3 bar to 3 bar for the same range of NETP.

3.3. Hydrophobic interaction

In the batch adsorption experiments, different IgG concentrations were equilibrated with the solid phase and the equilibrium concentration c_{IgG} of the liquid phase (supernatant) was analyzed.

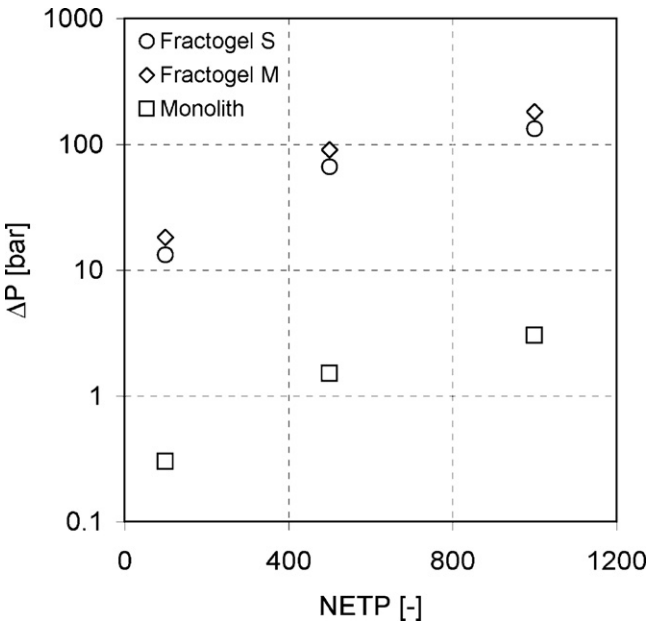

Fig. 6. Pressure drop as a function of NETP for monolith and Fractogel® EMD SO_3^- (S) and (M).

The IgG concentration in the adsorbed phase q_{IgG} was calculated by subtracting the IgG concentration in the supernatant from the initial IgG concentration. The obtained adsorption isotherms are shown inFig. 7. The experiments were carried out under 2 different adsorption conditions, namely a salt concentration of the liquid phase of 0.5 M $(NH_4)_2SO_4$ and 1 M $(NH_4)_2SO_4$ respectively. Assuming a Langmuir isotherm, the saturation capacities of the material are 132 mg/g and 149 mg/g, respectively. Even if the specific surface area (determined by N_2 adsorption) of the monolith is comparatively low it shows a high capacity for protein adsorption compared to classical bead materials. This can be explained by considering that the large specific surface area of porous materials produced with porogens is a result of a non-negligible amount of micropores, which are unaccessible for high molecular weight molecules

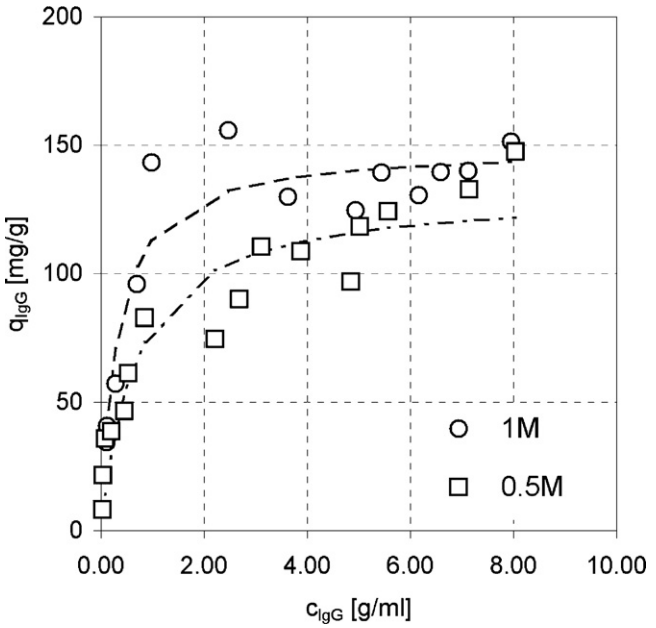

Fig. 7. Adsorption isotherms at two different buffer salt concentrations obtained by batch adsorption experiments.

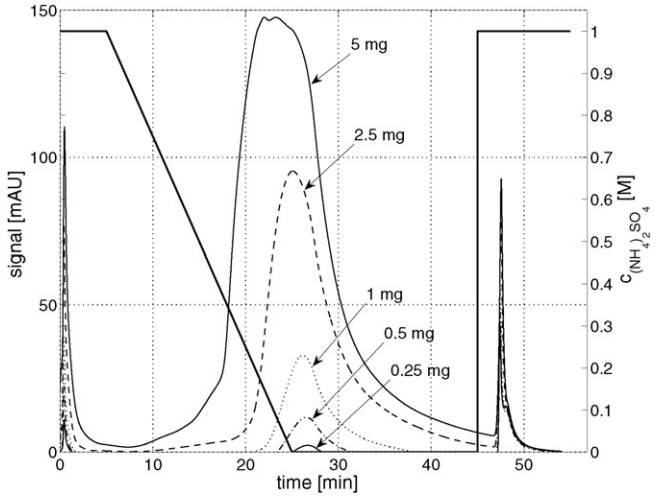

Fig. 8. Overloaded peak injections of IgG and desorption under salt gradient (bold line) elution.

like proteins. The results of the batch adsorption experiments lead to the conclusion that most of the surface area of the material produced by Reactive Gelation is accessible to large molecules.

To evaluate the hydrophobic interaction under chromatographic conditions, different amounts of IgG were injected under adsorbing conditions (1 M $(NH_4)_2SO_4$). To desorb the protein the salt concentration of the buffer was decreased to 0 in 20 min (14 column volumes). As shown in Fig. 8, the more IgG is adsorbed on the monolith, the higher the salt concentration, where desorption starts. This behavior can be explained using the equilibrium data shown in Fig. 7. At high solute concentration, adsorption capacity is strongly affected by salt concentration. Therefore, a significant desorption is taking place since the beginning of the salt gradient in the eluent and the left front of the peak os leaving the column sooner the larger the injected solute amount. On the other hand, adsorbed concentrations are almost independent of salt concentration at low solute concentration: therefore, the right part of the peak is leaving the column always at the same time, being the peak area decreasing with the injected solute amount. Finally, to check, if irreversible protein adsorption is taking place on the surface the same peak injections were repeated without a column and the peak areas of these experiments were compared to those of the gradient elution experiments. No significant difference of the peak areas could be observed, i.e. the protein adsorption on the surface is fully reversible.

4. Conclusion

The Reactive Gelation Process, previously applied to polystyrene latexes, was exploited here to prepare polymethylmethacrylate monoliths. These exhibited a much better mechanical resistance than the previously synthesized polystyrene monoliths. The size exclusion effect of these monoliths is higher than for the polystyrene material but it is still negligible compared to conventional bead material. The permeability is comparable in both materials and it is much better than the permeability of a packed bed with the same column efficiency. The most important result is that the polymethylmethacrylate monolith is not loosing efficiency with increasing velocity, which means, that convection is the predominant mass transport phenomenon. In addition, the column efficiency is 10 times better than the polystyrene monolith and 100 times higher than conventional bead material (Fractogel® EMD SO_3^-). For hydrophobic interaction chromatography the monolith prepared in this work shows a high capacity in batch adsorption experiments. Under chromatographic conditions the adsorbed protein fully desorbs while applying a salt gradient. This material was intended to become a matrix for ion exchange materials; however the P(MMA-co-EDM) material can be already used for HIC as a capture purification step in the downstream process.

References

[1] N. Marti, F. Quattrini, A. Butte, M. Morbidelli, Macromol. Mater. Eng. 290 (4) (2005) 221.
[2] M. Leonard, J. Chromatogr. B 699 (1–2) (1997) 3.
[3] G. Guiochon, J. Chromatogr. A 1168 (2007) 101.
[4] F. Svec, J. Sep. Sci. 27 (17–18) (2004) 1419.
[5] O. Okay, Prog. Polym. Sci. 25 (6) (2000) 711.
[6] S. Hjerten, J.L. Liao, R. Zhang, J. Chromatogr. 473 (1) (1989) 273.
[7] F. Svec, J.M.J. Frechet, Anal. Chem. 64 (7) (1992) 820.
[8] N. Vervoort, P. Gazil, G.V. Baron, G. Desmet, Anal. Chem. 75 (4) (2003) 843.
[9] E.C. Peters, F. Svec, J.M.J. Frechet, Chem. Mater. 9 (8) (1997) 1898.
[10] M. Lattuada, H. Wu, P. Sandkuhler, J. Sefcik, M. Morbidelli, Chem. Eng. Sci. 59 (8–9) (2004) 1783.
[11] P. Meakin, Adv. Colloid Interface Sci. 28 (4) (1988) 249.
[12] A. Rudin, The Elements of Polymer Science and Engineering, 2nd ed., Academic Press, San Diego, 1999.
[13] A. Butte, ISPPP, 2007.
[14] J. Coupek, M. Krivakova, S. Pokorny, J. Polym. Sci. Symp. 42 (1) (1973) 185.
[15] A. Jungbauer, R. Hahn, J. Chromatogr. A 1184 (1–2) (2008) 62.
[16] J.A. Alduncin, J. Forcada, J.M. Asua, Macromolecules 27 (8) (1994) 2256.
[17] S. Brunauer, P.H. Emmett, E. Teller, J. Am. Chem. Soc. 60 (1938) 309.
[18] I. Halasz, K. Martin, Angew. Chem. Int. Ed. 17 (12) (1978) 901.
[19] G. Guiochon, S. Golshan Shirazi, A.M. Katti, Fundamentals of Preparative and Nonlinear Chromatography, Elsevier, Amsterdam, 2006.
[20] P.J. Flory, Principles of Polymer Chemistry, Cornell University Press, Ithaca, NY, 1953.
[21] J.J. Vandeemter, F.J. Zuiderweg, A. Klinkenberg, Chem. Eng. Sci. 5 (6) (1956) 271.
[22] G. Carta, A.R. Ubiera, T.M. Pabst, Chem. Eng. Technol. 28 (11) (2005) 1252.
[23] R.V. Hogg, J.W. McKean, A.T. Craig, Introduction to Mathematical Statistics, 6th ed., Pearson Education, Upper Saddle River, NJ, 2005.
[24] E.N. Lightfoot, J.L. Coffman, F. Lode, Q.S. Yuan, T.W. Perkins, T.W. Root, J. Chromatogr. A 760 (1) (1997) 139.
[25] H. Darcy, Les Fontaines Publiques de a Ville de Dijon, Dalmont, Paris, 1856.
[26] N.A. Forrer, A. Butte, M. Morbidelli, J. Chromatogr. A 1214 (2008) 59.
[27] J.D. Bernal, J. Mason, Nature 188 (4754) (1960) 910.
[28] N. Marti, PhD thesis, ETH Zurich, 2007.